

From Hydrophobic to Hydrophilic Solvation: An Application to Hydration of Benzene

Pim Schravendijk and Nico F. A. van der Vegt*

Max-Planck-Institute for Polymer Research, Ackermannweg 10,
D-55128 Mainz, Germany

Received December 23, 2004

Abstract: We report a computer simulation study on the hydration of benzene, which, despite being hydrophobic, is a weak hydrogen bond acceptor. The effect of benzene–water hydrogen bonding on the hydration free energy has been analyzed in terms of solute–solvent energies and entropies. Our calculations show that benzene–water hydrogen bonding restricts the number of arrangements possible for the water molecules resulting in a more unfavorable (negative) solute–solvent entropy change than observed for a ‘nonpolar benzene’ not capable of accepting water hydrogen bonds. More favorable hydration free energies of aromatic hydrocarbons in comparison with aliphatic hydrocarbons observed experimentally as well as in our calculations must therefore be a result of more favorable solute–solvent interaction energies. This result supports the view that lower aqueous solubilities of nonpolar molecules compared to polar molecules are due to a lack of favorable electrostatic interactions with water molecules. The calculated hydration free energy, enthalpy, entropy, and hydration heat capacity of benzene are in good agreement with experimentally reported values.

1. Introduction

A detailed molecular understanding of hydration of hydrophobic and hydrophilic molecules is of prime importance in physical chemistry and biology. Most studies reported in the literature are devoted to hydrophobic hydration, which is believed to play an important role in protein folding and other self-assembly processes in water.^{1–5} Hydrophobic hydration of nonpolar solutes (i.e. aliphatic hydrocarbons), defined as the process of transferring the solute molecule from the gas phase into room-temperature water, is characterized by unfavorable (negative) hydration entropies and favorable, but smaller in magnitude, hydration enthalpies (negative). In room-temperature water, first shell water molecules form a hydrogen bonded cage structure surrounding the nonpolar solute. In a cage structure, the water molecules do not “waste” hydrogen bonds by pointing them at the solute; instead they orient their O–H bonds tangential to the solute surface in order to maximize hydrogen bonding with vicinal water molecules.⁵ Historically, Frank and Evans⁶ proposed

that the large entropy that opposes solute transfer into water arises from the cost of ordering the waters in this way.

The mechanism causing hydrophobicity of aromatic hydrocarbons (i.e. benzene, toluene) has a different nature than that causing the hydrophobicity of aliphatic hydrocarbons. In the case of aromatic hydrocarbons the enthalpic contribution predominates over the entropic contribution to the Gibbs energy of hydration.⁷ This results in a negative value of the hydration Gibbs energy of aromatic hydrocarbons, in contrast to the positive values obtained in the case of aliphatic hydrocarbons. In terms of aqueous solubilities, these differences cause the solubility of, e.g., *n*-hexane being almost 20 times lower than the solubility of benzene, although these hydrocarbons have similar molecular weight.⁸ Moreover, the heat capacity change upon transfer into aqueous solution (the thermodynamic hallmark that indicates the presence of structured hydration water), normalized to the water accessible surface area, is smaller for the aromatic hydrocarbons than the aliphatic ones.^{9,10}

Benzene is a slightly polar molecule due to the nature of its π -electron system that acts as a weak hydrogen bond acceptor.^{11–14} It has been argued that higher aqueous

* Corresponding author phone: +49 6131 379 245; fax: +49 6131 379 340; e-mail: vdervegt@mpip-mainz.mpg.de.

solubilities of aromatic hydrocarbons are probably due to formation of energetically favorable hydrogen bonds between the aromatic hydrocarbons and water.⁷ This explanation is in accord with the results of computer simulation studies using semiempirical force fields that showed that the hydration Gibbs energy of benzene can only be reproduced when adopting a model that includes a permanent charge distribution of benzene, which can be expressed by an electrostatic multipole expansion where the quadrupole moment is the first nonzero term.¹⁵ A consequence of this charge distribution is that the benzene–water potential energy is strongly dependent on the mutual orientation thereby accounting for weak hydrogen bonding interactions. Using available experimental and computer simulation data, Graziano and Lee¹⁶ however argued that the formation of weak O–H $\cdots\pi$ hydrogen bonds between water and benzene is likely to be largely enthalpy–entropy compensating therefore not explaining the higher solubility of aromatic hydrocarbons. Instead they argue that the large van der Waals interaction energy overwhelms the Gibbs energy cost of cavity formation at room temperature in contrast to aliphatic hydrocarbons where the Gibbs energy cost of cavity creation dominates.

In this paper, we report the hydration thermodynamics of benzene obtained by classical molecular dynamics simulations of benzene in simple point charge (SPC) water. To quantify how benzene–water hydrogen bonding changes the hydration thermodynamics, we studied a benzene model that favors formation of weak water–benzene hydrogen bonds (“real benzene”) as well as a “van der Waals benzene” model obtained by removing all partial charges of the first model while keeping the exchange repulsion and dispersion interaction terms unaffected. In addition to calculating the Gibbs energy of hydrating the real benzene and van der Waals benzene models, we calculated the enthalpy, entropy, and heat capacity of hydration. To understand the difference in aqueous solubility between the two benzene models better, we also studied contributions to the hydration enthalpy and entropy arising from benzene–water interactions (the solute–solvent interaction energy and solute–solvent entropy) and reorganization of the solvent.

2. Thermodynamics

The solute hydration free energy (the Ben-Naim pseudo-chemical potential¹⁷ $\mu_{ex,S}$) and the corresponding hydration enthalpy ($h_{ex,S}$) and entropy ($s_{ex,S}$) have been theoretically analyzed by Yu and Karplus¹⁸ who showed that

$$\mu_{ex,S} = \Delta u_{SW} - T\Delta s_{SW} \quad (1)$$

$$(h_{ex,S})_P = \Delta u_{SW} + (\Delta h_{WW})_P \quad (2)$$

$$(s_{ex,S})_P = \Delta s_{SW} + (\Delta h_{WW})_P/T \quad (3)$$

In eqs 1–3, Δu_{SW} denotes the energy of solute–water interaction (the solute–solvent energy), Δs_{SW} denotes the entropy change of solute–water interaction (the solute–solvent entropy), and $(\Delta h_{WW})_P$ denotes the (constant pressure) water–water enthalpy change (solvent reorganization enthalpy). The derivation of eqs 1–3 and a discussion of the

solute–solvent entropy are presented in more detail in the Appendix. Whereas $\mu_{ex,S}$ is ensemble independent, $h_{ex,S}$ and $s_{ex,S}$ do depend on the insertion condition (constant P, T ; constant V, T) with the ensemble dependence occurring in the Δh_{WW} term.^{19,20} Here we restrict ourselves to conditions of constant pressure and temperature at which experiments are usually performed and drop the subscript $(\cdots)_P$. In computer simulation studies, $\mu_{ex,S}$ may be obtained by thermodynamic integration (TI), perturbation (TP), or related methods.²⁰ Since Δu_{SW} is obtained straightforwardly by keeping an average of the solute–water interaction energy at the end-point simulation ($\lambda=1$) in TI/TP, Δs_{SW} follows directly from eq 1. We note that both Δu_{SW} and Δs_{SW} are negative (see the Appendix), while Δh_{WW} is positive. Eqs 1–3 have several important consequences:

(i) The water–water enthalpy change has no impact on $\mu_{ex,S}$. In hydrophobic hydration, Δh_{WW} is usually small (in comparison to solvent reorganization energies in organic solvents) and positive²¹ because water hydrates nonpolar solutes without significantly sacrificing hydrogen bonding.

(ii) Cancellation of Δh_{WW} in $\mu_{ex,S}$ ($= h_{ex,S} - Ts_{ex,S}$) does not mean that the extent to which water–water hydrogen bonds are disrupted is irrelevant in understanding $\mu_{ex,S}$ because Δu_{SW} and Δs_{SW} are defined as ensemble averages containing the water–water interaction implicitly.¹⁸ The solute–solvent entropy change ($-T\Delta s_{SW}$) can conceptually be interpreted as the free energy to create a solute cavity that has all solvent molecules properly oriented to accommodate all chemical moieties of the solute,²² while the solute–solvent energy (Δu_{SW}) may be interpreted as the remaining solute–cavity interaction contribution to $\mu_{ex,S}$. In hydrophobic hydration, first shell water molecules orient to minimize their loss of H-bonds. Any reduction of orientational entropy associated with preferred water orientations (driven by W–W interactions) therefore appears in Δs_{SW} . The cavity formation work ($-T\Delta s_{SW}$) also increases with the excluded volume radius (i.e. loss of translational entropy).

(iii) In hydrophilic hydration, polar solute–solvent interactions (e.g. dipolar interactions, dipole–quadrupole interactions) bias orientations of hydration waters, too. This process may in fact reduce the solute–solvent entropy stronger than the biasing of water orientations close to nonpolar solutes. In that case, lower aqueous solubilities of nonpolar molecules over polar molecules result from a lack of favorable electrostatic interactions with the solvent.

3. Computational Details

Thermodynamic Calculations. Excess chemical potentials were calculated by TI using at least 50 λ -values. At each new λ , the system was first equilibrated for 50 ps after which the free energy derivative was sampled for 500 ps. A soft-core λ scaling was used²³ to avoid singularities of the derivative at the end-points. The excess partial molar enthalpy was calculated using the expression

$$h_{ex,S} = \langle U_{SW} + U_{WW} + PV \rangle_{\text{solution}} - \langle U_{WW} + PV \rangle_{\text{pure H}_2\text{O}} \quad (4)$$

where U_{SW} denotes the solute–water interaction energy, U_{WW} denotes the sum of interaction energies of the water

Table 1. Nonbonded Interaction Parameters^a

atom	$C_{12}(i,j)$ (10^{-6} kJ mol ⁻¹ nm ¹²)	$C_6(i,j)$ (10^{-3} kJ mol ⁻¹ nm ⁶)	q_i (e)
Benzene (GROMOS 43A1) ²⁶			
C	3.374569	2.340624	-0.10
H	0.015129	0.084640	0.10
Benzene (GROMOS 53A6) ²⁷			
C	4.937284	2.340624	-0.14
H	0.015129	0.084640	0.14
SPC Water ²⁵			
O	2.634129	2.617346	-0.82
H	0.00	0.00	0.41

^a Nonbonded interaction function: $V(r_{ij}) = C_{12}(i,j)/r_{ij}^{12} - C_6(i,j)/r_{ij}^6 + q_i q_j / 4\pi\epsilon_0 [1/r_{ij} + (\epsilon_{RF} - 1)r_{ij}^2 / (2\epsilon_{RF} + 1)R_C^3 - 3\epsilon_{RF} / (2\epsilon_{RF} + 1)R_C]$. R_C : long-range cutoff radius. ϵ_{RF} : reaction field relative dielectric permittivity. Combination rules: $C_6(i,j) = C_6(i,i)^{1/2} C_6(j,j)^{1/2}$; $C_{12}(i,j) = C_{12}(i,i)^{1/2} C_{12}(j,j)^{1/2}$.

molecules with all other water molecules, and PV denotes a pressure–volume work term. The brackets denote a constant pressure–temperature ensemble average. Two constant pressure–temperature simulations, one of the aqueous solution (1 solute, N solvent molecules) and one of the neat solvent (N solvent molecules), are performed, and the average potential energies are subtracted (the $P\Delta V$ term is usually small). Because both terms on the right-hand side of eq 4 are of $O(N)$ whereas $h_{ex,S}$ is of $O(1)$, the statistical accuracy obtained in MD runs of several hundreds of picoseconds is usually poor. We produced long (90 ns) trajectories to sample the two averages in eq 4 resulting in statistical inaccuracies of $h_{ex,S}$ smaller than 0.3 kJ/mol. Excess partial molar entropies were obtained from the calculated excess chemical potential and enthalpy using $Ts_{ex,S} = h_{ex,S} - \mu_{ex,S}$. Solute–solvent entropies were obtained from the calculated excess chemical potential and solute–solvent energy using $T\Delta s_{SW} = \Delta\mu_{SW} - \mu_{ex,S}$ (eq 1). The solute–solvent energy was obtained from the simulations by taking the average benzene–water interaction energy. Heat capacities of hydration were calculated from the temperature dependence of $h_{ex,S}$ using the finite difference expression

$$c_{P,ex,S}(T) = \frac{h_{ex,S}(T + \Delta T) - h_{ex,S}(T - \Delta T)}{2\Delta T} \quad (5)$$

A temperature difference $\Delta T = 20$ K was chosen in our simulations. The excess partial molar enthalpies $h_{ex,S}(T + \Delta T)$ and $h_{ex,S}(T - \Delta T)$ were calculated using eq 4 based on 90 ns trajectories. The statistical inaccuracy of $c_{P,ex,S}$ is determined by that of $h_{ex,S}$ and amounts to 15–20 J mol⁻¹ K⁻¹.

Simulation Details. All simulations were performed using the Gromacs 3.2.1 simulation package^{23,24} and were based on an equilibrated cubic, periodic simulation box containing 1500 water molecules and 1 benzene molecule. The simple point charge (SPC) model of water was used.²⁵ Benzene was modeled using the GROMOS 43A1 force field parameters.²⁶ For reasons of comparison, we used the recent GROMOS 53A6 parameters as well.²⁷ The nonbonded force field parameters are summarized in Table 1. For the bonded parameters, which are identical in the 43A1 and 53A6

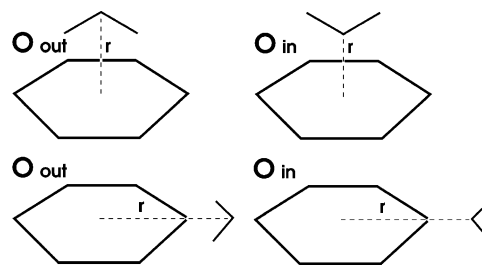


Figure 1. Relative orientations used for calculating the water–benzene interaction. The distance r is defined between the water oxygen and the ring center of mass. In orientation O_{out} , the water dipole moment is pointing toward the solute, in orientation O_{in} the water dipole moment is oriented outward.

GROMOS force fields, we refer to refs 26 and 27. Intramolecular Lennard-Jones and electrostatic interactions were accounted for between atom pairs separated by more than 3 bonds. The simulation temperature was kept constant at 302 K by weakly coupling to a temperature bath with a relaxation time of 0.1 ps.²⁸ The pressure was maintained at 1 atm by also applying the weak coupling algorithm with a relaxation time of 0.5 ps and an isothermal compressibility of 45.75×10^{-5} (kJ mol⁻¹ nm⁻³)⁻¹. The equilibrated box length was 3.592 nm. For nonbonded interactions, a twin-range method with cutoff radii of 0.8 and 1.4 nm was used. Outside the longer cutoff radius a reaction field correction was applied with a relative dielectric permittivity of 54.0. The integration time step was 2 fs, and the pairlist for pairs within the inner cutoff and the energies and forces for pairs between the inner and outer cutoff radii were updated every 10 fs. All bond lengths were kept constant using the SHAKE algorithm²⁹ using a relative geometrical tolerance of 10^{-4} .

Benzene–Water Interaction. The benzene–water interaction potential is strongly orientation dependent. Based on the relative orientations shown in Figure 1, we calculated the interaction energy between a benzene–water (SPC) pair as a function of the distance r defined in Figure 1 (using the GROMOS 43A1 parameters in Table 1). Figure 2 shows the corresponding potential energy curves (denoted “real O in” and “real O out”), which also includes the interactions obtained when not accounting for the electrostatic part of the interaction (denoted “van der Waals O in & O out”). The interaction energies for a water molecule oriented perpendicular to the aromatic plane (Figure 2a) are in good agreement with the energies reported by Linse,^{30,31,12} which are based on ab initio quantum chemical calculations using a Hartree–Fock self-consistent-field approximation combined with a second-order perturbation procedure to account for the dispersion energy. The dashed line in Figure 2a (“real O out”; benzene–water hydrogen bonding) shows a minimum at approximately 3.0 Å with a corresponding energy between 13 and 14 kJ/mol. In the ab initio study,^{30,31,12} the minimum is found at the same distance with an energy of 12–13 kJ/mol. The configuration with the oxygen pointing inward (dotted curve in Figure 2a) is repulsive and is also in good agreement with the corresponding ab initio benzene–water interaction reported in ref 12. For conformations where the water is aligned in the benzene plane (Figure 2b), the agreement between our data and those from the work of

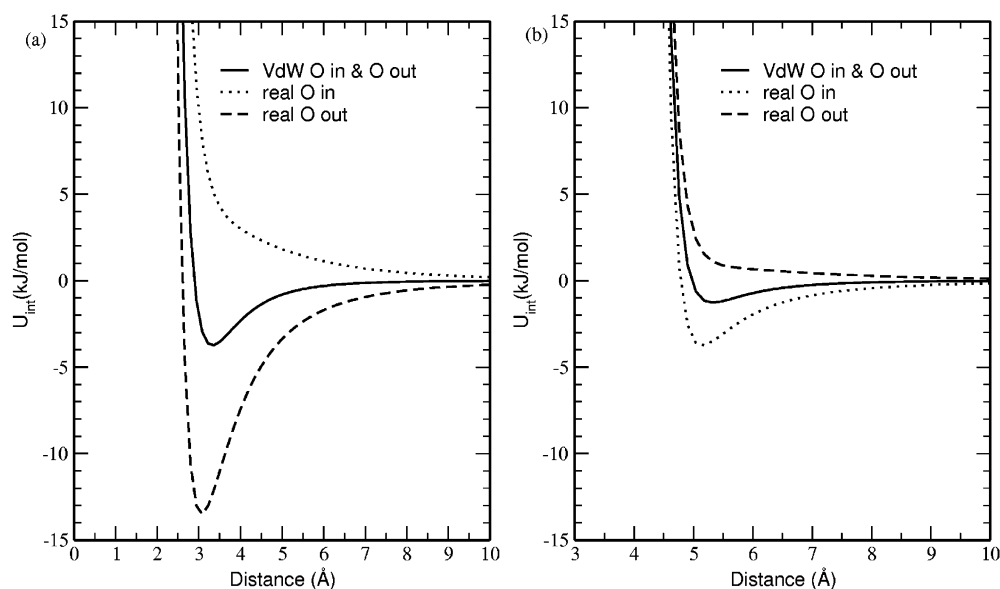


Figure 2. Potential energy curve for SPC water–benzene interaction. (a) The water molecule is located above the benzene plane. (b) The water molecule is located in the plane of the benzene ring (see Figure 1). Solid line, van der Waals benzene (the quadrupole–dipole interaction is omitted); dashed line, water having its dipole pointing inward; and dotted line, water having its dipole pointing outward (see Figure 1).

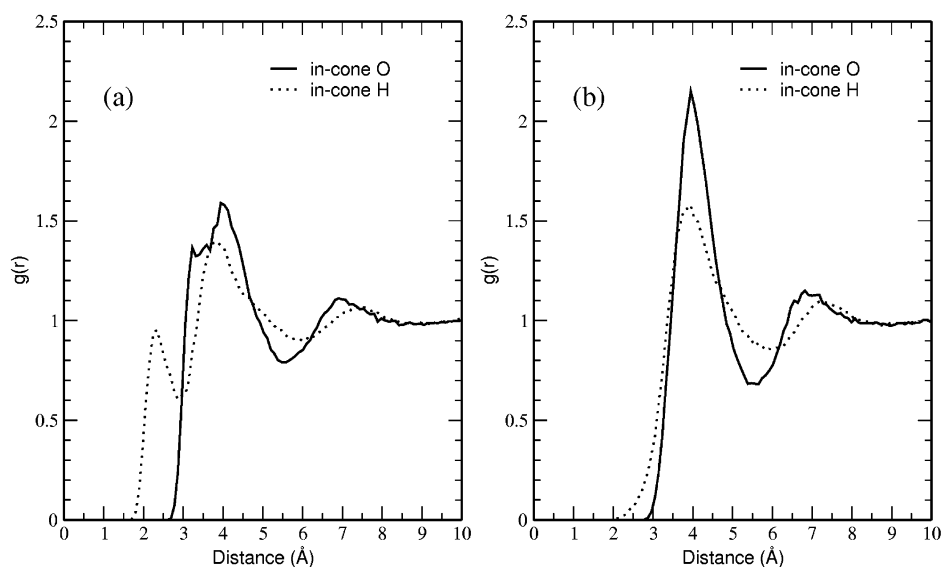


Figure 3. In-cone benzene–water radial distribution functions. Solid line, benzene center-of-mass-to-water oxygen RDF and dashed line, benzene center-of-mass-to-water hydrogen RDF. (a) Real benzene. (b) van der Waals benzene.

Linse et al. is less satisfactory. In the *ab initio* study, the energy minimum for the oxygen-inward conformation is found around 4.5 Å with a corresponding energy of 7–8 kJ/mol, while with the GROMOS 43A1 force field this minimum is located at 5.2 Å with a corresponding energy of 3.6 kJ/mol. For the configuration with the oxygen pointing outward, the *ab initio* data show a slightly stronger repulsion than our data.

4. Results and Discussion

4.1. Hydration Structure. Radial Distribution Functions.

Due to the anisotropic benzene–water interaction potential, the benzene hydration structure should preferably be characterized by distinguishing water molecules inside the volume above the benzene plane from water molecules

located elsewhere. We adopted the approach of Linse et al.³¹ to subdivide the space around the benzene. Water molecules inside the conical volumes above and below the benzene plane and remaining water molecules were considered separately. The cones make a 45° angle with the benzene symmetry axis. Water molecules located inside the conical volumes are hydrogen bonded to benzene more likely than molecules located outside. Figure 3 shows the in-cone water–benzene center of mass radial distribution function (RDF) for real benzene (Figure 3a), modeled with the GROMOS 43a1 parameters, and the van der Waals benzene model (Figure 3b). For the case of the real benzene, the first peak of the hydrogen at 2.25 Å clearly indicates that water donates hydrogen bonds to benzene. The peak area up to 3 Å corresponds to 1.0 benzene–water hydrogen bonds. The

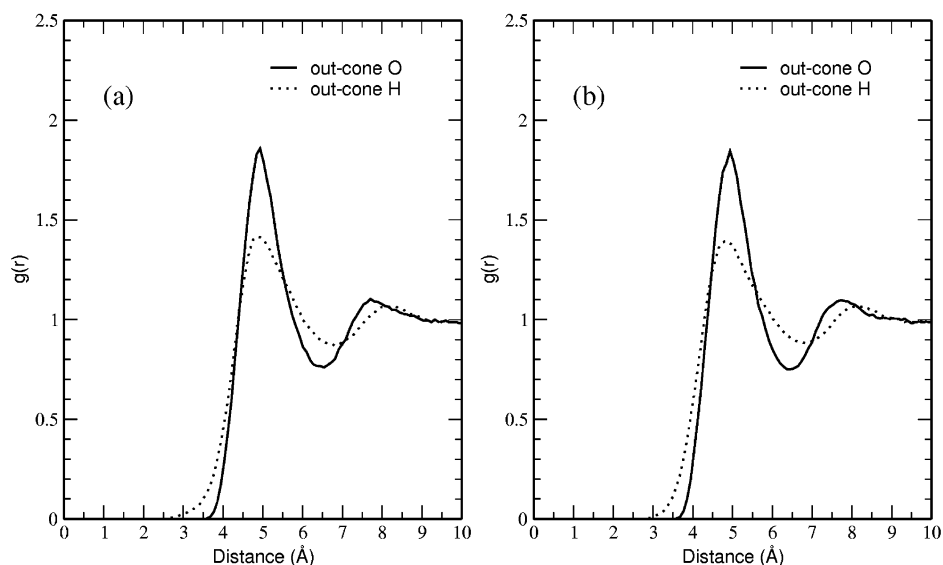


Figure 4. Out-of-cone benzene–water radial distribution functions. Solid line, benzene center-of-mass-to-water oxygen RDF and dashed line, benzene center-of-mass-to-water hydrogen RDF. (a) Real benzene. (b) van der Waals benzene.

larger oxygen peak is split in two parts. The first maximum occurs at 3.25 Å and corresponds to the water molecule donating a hydrogen bond to benzene (i.e. the distance between the first maximum of the hydrogen RDF and that of the oxygen RDF is exactly a OH bond length). The second oxygen peak at 4 Å corresponds to water not directly hydrogen bonded to benzene. The incone RDFs for the van der Waals benzene (Figure 3b) are typical of hydrophobic hydration. The peaks are narrower and the maxima are higher compared to the real benzene system, indicating significantly more structured hydration water. Moreover, the first maximum for the oxygen and hydrogen RDFs is located at the same distance, which suggests that water orients one of its OH bonds parallel to the surface of the nonpolar solute. The first peak of the hydrogen RDF has a broad shoulder extending to larger distances, which arises from the second OH bond that orients toward the bulk where it donates a hydrogen bond to water molecules in the second solvation shell. The latter becomes apparent from the second maximum of the oxygen RDF being located closer to the solute than the second maximum of the hydrogen RDF. The out-of-cone RDFs for real benzene and van der Waals benzene are shown in Figure 4 (parts a and b, respectively). For both systems the observed structure is typical of hydrophobic hydration with no significant differences between the realistic and van der Waals benzene models.

Orientalional Distributions. The probability density of orientation of the water OH bonds with respect to the vector connecting the benzene center of mass and the water oxygen is shown in Figure 5. The data apply to water molecules in the first shell ($r < 6$ Å), which on average contains 26.5 molecules. No distinction is made here between water molecules located inside or outside the conical volumes. The distribution $P'(\theta)$ obtained just from the statistical sampling of the angles was rescaled according to $P(\theta) = P'(\theta)/\sin \theta$, accounting for the volume elements associated with the angle θ . For the GROMOS 43A1 van der Waals model, we observe a higher occurrence of OH orientation at both 0° (radially outward) and 110–120°. Postma et al.³² made similar

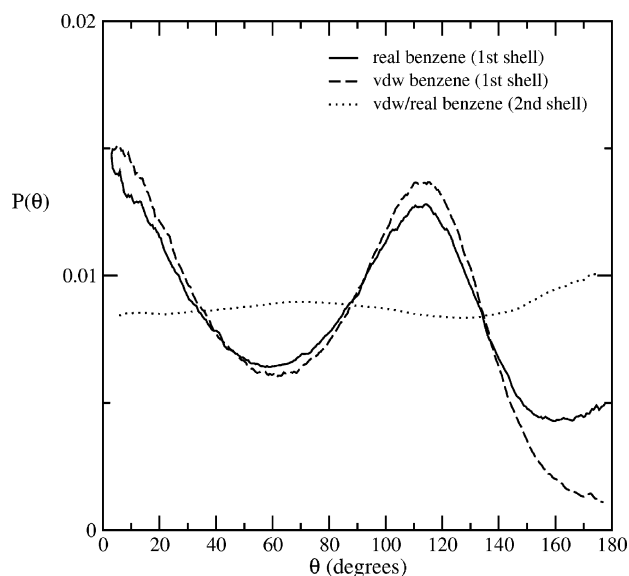


Figure 5. Probability density of orientation of the OH direction with respect to the vector connecting the benzene center of mass and water oxygen (normalization: $\int P(\theta) \sin \theta d\theta = 1$). Data apply to molecules in the first shell ($r < 6$ Å) or second shell ($6 < r < 9$ Å). Solid line, real benzene (first shell); dashed line, van der Waals benzene (first shell); and dotted line, benzene (second shell).

observations in a study of the hydration of spherical cavities with a thermal radius of 3 Å (the orientationally averaged cavity radius of van der Waals benzene equals ~ 3.5 Å). They showed that water molecules may have one OH-bond directed toward the bulk, whereas the other OH bond is directed parallel to the cavity surface, but may also have both of their OH-bonds parallel to the cavity surface. The water orientational distribution corresponding to real benzene shows somewhat weaker maxima at 0° and 110° and has an additional weak maximum at 180° (OH radially inward), which arises from benzene–water hydrogen bonding. The orientational distribution of second shell hydration waters (dotted line in Figure 5) neither reveals strong preferential

Table 2. Hydration Thermodynamics of Benzene and “van der Waals Benzene”^a

<i>T</i> (K)	$\mu_{ex,S}$ (kJ/mol)	$h_{ex,S}$ (kJ/mol)	$S_{ex,S}$ (J/mol/K)	$C_{p,ex,S}$ (J/mol/K)
Experimental ^b				
278		−35.7	−108.4	318.8
298	−3.6	−29.6	−87.2	291.6
323		−22.6	−64.6	268.1
43A1 Benzene				
282		−32.7		
302	−4.8	−29.3	−82.2	277.5
322		−21.6		
53A6 Benzene				
282		−34.5		
302	−6.7	−31.1	−81.8	217.5
322		−25.8		
43A1 Benzene, van der Waals Only				
282		−29.7		
302	1.0	−24.8	−86.5	327.5
322		−16.6		

^a The excess chemical potentials ($\mu_{ex,S}$) were computed by thermodynamic integration, and the excess partial molar enthalpies ($h_{ex,S}$) were computed using eq 4 in which total potential energies of the solution (water + benzene) and solvent (water) MD simulations were averaged over 90 ns time periods. The excess partial molar entropies ($S_{ex,S}$) were obtained from $T S_{ex,S} = h_{ex,S} - \mu_{ex,S}$. Heat capacity changes ($C_{p,ex,S}$) were calculated by finite difference (eq 5). ^b Experimental values were from ref 7.

OH directions nor does it show differences for the real and van der Waals solutes.

4.2. Hydration Thermodynamics. In Table 2 all thermodynamic hydration quantities are summarized. For real benzene, the calculations were performed using the 43A1²⁶ and 53A6²⁷ GROMOS parameters (see Table 1). The thermodynamic quantities for van der Waals benzene were obtained from simulations using 12–6 Lennard-Jones parameters from the 43A1 force field. The best agreement with the experimental data is found for the 43A1 GROMOS parameter set and will be discussed here. Not only the benzene excess chemical potential agrees satisfactorily with the experimentally reported value but also the excess partial molar enthalpy and entropy are closely reproduced. Especially the latter quantities provide a good test of the quality of a particular force field. Although the excess chemical potential can be predicted correctly, it may happen for the wrong reason because errors in the energy may cancel out against errors in the entropy. The isobaric heat capacity of benzene hydration is predicted most accurately as well with the GROMOS 43A1 force field. The hydration thermodynamics of the van der Waals benzene model differs from the real model and is typical of hydrophobic hydration: the excess chemical potential is positive and also the isobaric heat capacity of hydration is significantly more positive than for real benzene. The excess partial molar entropies of van der Waals and real benzene do not significantly differ. The excess partial molar enthalpy of real (43A1) benzene is however −4.5 kJ/mol more favorable compared to that of van der Waals benzene, hence the larger negative excess chemical potential of real benzene is mainly enthalpic. This enthalpy difference compares with a value of −5.4 kJ/mol

Table 3. Solute–Solvent Energy Change (Δu_{SW}), Solute–Solvent Entropy Change ($T\Delta s_{SW}$), and Solvent Reorganization Energies (Δh_{WW}) for Hydrating Real Benzene and van der Waals Benzene

<i>T</i> (K)	Δu_{SW} (kJ/mol)	$T\Delta s_{SW}$ (kJ/mol)	Δh_{WW} (kJ/mol)
43A1 Benzene			
282	−61.2		28.5
302	−59.4	−54.6	30.1
322	−57.5		35.9
43A1 Benzene, van der Waals Only			
282	−47.1		17.4
302	−45.6	−46.6	20.8
322	−43.9		27.3

predicted by Makhatadze and Privalov⁷ based on combining experimental data for benzene and aliphatic hydrocarbons, the latter corrected for the benzene accessible surface area. Based on a similar calculation, Makhatadze and Privalov predict a change of the excess chemical potential and excess partial molar entropy of −13.4 kJ/mol and +26.8 J/mol/K, respectively, which our calculations do not reproduce.

Solute–Solvent Contributions. The solute–solvent energies, Δu_{SW} , solute–solvent entropies, $T\Delta s_{SW}$, and water reorganization enthalpies, Δh_{WW} , are shown in Table 3 for the 43A1 real benzene and the 43A1 van der Waals benzene models. The benzene–water energy is −13.8 kJ/mol more favorable than the van der Waals benzene–water energy ($T = 302$ K). Because benzene on average accepts one hydrogen bond from water and the benzene–water hydrogen bond energy equals approximately 13 kJ/mol (Figure 2a), this result is expected.

The enthalpy change of water reorganization was calculated based on eq 4, which can also be written as

$$\begin{aligned}
 h_{ex,S} &= \langle U_{SW} \rangle_{\text{solution}} + \\
 &\quad [\langle U_{WW} + PV \rangle_{\text{solution}} - \langle U_{WW} + PV \rangle_{\text{pure H}_2\text{O}}] \\
 &= \Delta u_{SW} + \Delta h_{WW}
 \end{aligned}
 \quad (6)$$

The water reorganization enthalpies (Δh_{WW}) are large and positive contributing significantly to the excess partial molar enthalpies. For dissolving a solute in its own pure liquid at constant P and T , the solvent reorganization enthalpy equals the average potential energy of the liquid.³³ Transferring for example a SPC water molecule from the saturated vapor phase into the liquid SPC water phase involves a solvent reorganization enthalpy of 41.5 kJ/mol at 298 K. For benzene (43A1 model) in its own liquid this enthalpy is 33.2 kJ/mol. If one compares these numbers to the reorganization enthalpies in Table 3 it shows that, in particular for van der Waals benzene, the water reorganization enthalpy is small. For the real benzene model, Δh_{WW} is larger because benzene–water hydrogen bonding happens at the expense of water–water hydrogen bonding.

The temperature dependencies of Δu_{SW} and Δh_{WW} are interesting because they provide further clues on the different heat capacity changes of real and van der Waals benzene (Table 2). In the 40 K temperature interval, Δu_{SW} increases with 3.7 and 3.2 kJ/mol for real and van der Waals benzene,

respectively. For the real benzene model we found that this energy change was almost exclusively due to a reduction of the benzene–water van der Waals energy with increasing temperature. The benzene–water electrostatic interactions changed only little (+0.7 kJ/mol) in this temperature interval. Interestingly, in the same temperature interval, Δh_{ww} increases with 7.4 kJ/mol (real benzene) and 9.9 kJ/mol (van der Waals benzene). Based on these energy changes it can be concluded that the larger positive heat capacity change of hydrating van der Waals benzene is entirely due to an increase of the water–water enthalpy, which occurs upon “melting” the cagelike water structure surrounding the nonpolar solute. We note that under conditions of constant pressure, theoretical work¹⁹ and experimental data³⁴ have suggested that the mechanism of enthalpy absorption may indeed be localized in the solute hydration shell (whereas under conditions of constant volume, the excess partial molar energy contains a nonlocal, bulk response contribution).¹⁹

It is interesting to address in some detail the question to what extent reorganization of the solvent occurring in response to introducing solute–solvent electrostatic interactions is enthalpy–entropy compensating in the free energy. Because the solute molecule considered here is rigid all the entropy change of this process is due to the rearrangement of solvent molecules. Thus, as originally proposed by Lee,³⁵ the total entropy change can be considered as the solvent reorganization entropy. We will refer to this quantity as Δs^{reo} ($= s_{ex,s}(\text{real}) - s_{ex,s}(\text{vanderWaals})$). The corresponding solvent reorganization enthalpy we refer to as Δh^{reo} ($= \Delta h_{ww}(\text{real}) - \Delta h_{ww}(\text{vanderWaals})$). The free energy change of introducing solute–solvent electrostatic interactions contains the free energy of solvent reorganization ($\Delta h^{reo} - T\Delta s^{reo}$) in addition to the change of solute–solvent interaction energy. In case perfect enthalpy–entropy compensation occurs ($T\Delta s^{reo} = \Delta h^{reo}$), the free energy change of introducing the electrostatic interactions will only be determined by the change of the solute–solvent interaction energy. The solute–solvent energy change (Table 3) amounts to $-59.4 + 45.6 = -13.8$ kJ mol⁻¹. The free energy change (43A1 benzene, Table 2) is however smaller and amounts to $-4.8 - 1.0 = -5.8$ kJ mol⁻¹ indicating that solvent reorganization contributes unfavorably to the free energy change. From Table 2 we see that introducing benzene–water electrostatic interactions causes an entropy change $T\Delta s^{reo} = 1.3$ kJ mol⁻¹ (302 K). The reorganization enthalpy (Table 3) is significantly larger and amounts to $\Delta h^{reo} = 9.3$ kJ mol⁻¹. Solvent reorganization thus causes an (small) increase of the entropy, which is however overcompensated by a much larger unfavorable increase of the solvent reorganization enthalpy. In this view, the presence of weak solute–solvent hydrogen bonds forces the solvent to assume strained, less stable, conformations relative to the pure solvent leading to a free energy change smaller than the energy gained by solute–solvent hydrogen bonding.

Although we may just have reached a satisfactory conclusion, the microscopic significance of the reorganization entropy remains problematic. An alternative way exists to arrive the same conclusion based on a discussion of the solute–solvent entropy and the solute–solvent energy whose

microscopic significance is discussed in the Appendix. We start out by noting that a zero change of the solute–solvent entropy is the condition for perfect enthalpy–entropy compensation of the solvent reorganization process discussed above (i.e. $\Delta h^{reo} - T\Delta s^{reo} = T(\Delta s_{sw}(\text{real}) - \Delta s_{sw}(\text{vanderWaals}))$). In the Appendix we show³⁷

$$T\Delta s_{sw} = k_B T \ln P_{ins} - [(\langle \psi^2 \rangle - \langle \psi \rangle^2) \beta / 2 + \dots]_a \quad (7)$$

The solute–solvent entropy is determined by (1) the probability (P_{ins}) that in a system of only solvent molecules a cavity is found where the solute–solvent interaction energy (ψ) is attractive and (2) the fluctuations of the solute–solvent energy in configurations of the solute–solvent system where $\psi < 0$. The second contribution reflects the fact that fluctuations in positions and orientations of solvent molecules vicinal to the solute are biased by attractive solute–solvent interactions resulting in a reduction of configuration space and thus a reduction of the entropy. The process of introducing the electrostatic interactions leads to favorable change of Δu_{sw} of -13.8 kJ mol⁻¹ while causing a compensating unfavorable change of $T\Delta s_{sw}$ of $-54.6 + 46.6 = -8.0$ kJ mol⁻¹ (see Table 3). We note that this observed change of $T\Delta s_{sw}$ results from changes in the second term on the right-hand side of eq 7, not from changes in the first term: calculations of $(\langle \psi^2 \rangle - \langle \psi \rangle^2) \beta / 2$, using the 90 ns trajectories of hydrated real benzene and van der Waals benzene, resulted in $12.8 (\pm 0.2)$ kJ mol⁻¹ for real benzene and $3.9 (\pm 0.2)$ kJ mol⁻¹ for van der Waals benzene, thus contributing -8.9 kJ mol⁻¹ to the change of $T\Delta s_{sw}$. Benzene–water hydrogen bonding thus introduces a stronger bias on the orientations sampled by hydration waters than the bias introduced in hydrating nonpolar van der Waals benzene. The formation of weak benzene–water hydrogen bonds, which energetically favors the hydration of real benzene, happens in competition with solvent–solvent interactions that favor water–water hydrogen bonding. In creating these energetically favorable benzene–water hydrogen bonds, the solvent is forced to sacrifice some of its own hydrogen bonds. The corresponding water configurations will have a potential energy significantly larger than configurations representative of pure water and configurations compatible with hydrating van der Waals benzene (i.e. the solvent reorganization enthalpy is positive). Clearly, due to its attempt to maintain hydrogen bonds, pure water will with lower probability sample configurations representative for the hydration structure of real benzene than for van der Waals benzene. The probability $\exp[\Delta s_{sw}/k_B]$ to successfully insert real benzene in pure water configurations with an appropriately formed cavity (that satisfies benzene–water hydrogen bonding) will therefore be lower than the probability to successfully insert van der Waals benzene. We thus see that the reduction of the solute–solvent entropy arising by introducing electrostatic benzene–water interactions originates from less stable configurations that water has to adopt in order to donate hydrogen bonds to benzene. This automatically implies that the solvent reorganization process is noncompensating and the solvent reorganization enthalpy is positive.

We conclude by noting that moderately polar, real benzene dissolves better than van der Waals benzene due to energetically favorable electrostatic interactions with the solvent. Although here we have only shown that the hydration entropies of van der Waals and realistic benzene do not significantly differ, we more generally believe that lower aqueous solubilities of nonpolar compared to polar molecules are not due to the entropy differences but due to the lack of favorable electrostatic interactions with the solvent. This view, advocated earlier by Gallicchio et al.,³³ is supported by the Monte Carlo simulations of Stone et al.³⁶ based on which the authors conclude that poor aqueous solubilities correlate with poor solute–solvent interaction.

5. Conclusions

In this study we have used MD simulations to make a detailed comparison of the hydration structure and thermodynamics of a realistic benzene model capable of forming weak hydrogen bonds with water and a nonrealistic (van der Waals) benzene model incapable of accepting H-bonds. Calculations were performed using an all-atom benzene model taken from the GROMOS force field and the SPC water model. The benzene excess chemical potential and excess partial molar enthalpy and entropy as well as the hydration heat capacity change were calculated and showed good overall agreement with the corresponding experimental values. Our calculations indicate that a favorable hydration free energy of benzene compared to “van der Waals benzene” is due to favorable electrostatic (H-bonding) interactions with the solvent. The solvation entropies of the realistic and van der Waals benzene models were found to be not significantly different. The hydration heat capacity change of the van der Waals model was found larger than that of the realistic model, which could be assigned to a larger enthalpy absorbed by the hydration water of the van der Waals model. Although changes of water–water interactions greatly affect the hydration enthalpy, entropy, and heat capacity, they have no impact on the benzene solubility due to exact enthalpy–entropy compensation of the solvent reorganization enthalpy. Therefore, we also studied the solute–solvent energy and solute–solvent entropy, which are the pertinent quantities determining the chemical potential of the solute. The solute–solvent entropy of the van der Waals benzene model is larger (more favorable) than that of the realistic benzene model. This result indicates that restrictions in water orientations due to benzene–water hydrogen bonding are larger than restrictions in water orientations close to the van der Waals (hydrophobic) benzene. The low solubility of the nonpolar van der Waals benzene relative to real benzene therefore cannot be explained in terms of the entropy change but is due to lack of favorable electrostatic interactions with the solvent water molecules.

Acknowledgment. The authors thank Luigi Delle Site, Berk Hess, Kurt Kremer, and Christine Peter for useful discussions and comments regarding the manuscript.

Appendix: The Solute–Solvent Entropy

The solute–solvent terms in eq 1 have been analyzed by Sanchez et al.³⁷ whose treatment we briefly summarize

below. The reader is referred to ref 37 for the derivation of eq 12, which we do not repeat here. The solute (S) excess chemical potential ($\mu_{ex,S}$) can be defined using Widom’s potential distribution theorem³⁸

$$\begin{aligned}\mu_{ex,S} &= -\beta^{-1} \ln \langle e^{-\beta\psi} \rangle_0 \\ &= \beta^{-1} \ln \langle e^{\beta\psi} \rangle\end{aligned}\quad (8)$$

In eq 8, ψ denotes the interaction energy of the solute molecule with the other (solvent) molecules, $\beta = (k_B T)^{-1}$ with k_B the Boltzmann constant, and the angular brackets denote a constant volume–temperature ensemble average. The subscript zero indicates that the average is taken under the condition that the other molecules in the system do not sense the presence of the “test molecule”. The average without subscript indicates a normal ensemble average where the solute molecule interacts and influences the other system molecules. The excess chemical potential of molecules S (eq 8) is defined relative to an ideal gas with a number density of molecules S equal to the number density of the solution. Eq 8 can be decomposed in an energetic and entropic contribution

$$\begin{aligned}\mu_{ex,S} &= \beta^{-1} \ln \langle e^{\beta\psi} \rangle \\ &= \langle \psi \rangle + \beta^{-1} \ln \langle e^{\beta(\psi - \langle \psi \rangle)} \rangle \\ &\equiv \Delta u_{SW} - T \Delta s_{SW}\end{aligned}\quad (9)$$

In eq 9, $\Delta u_{SW} = \langle \psi \rangle$ and $\Delta s_{SW} = -k_B \ln \langle e^{\beta(\psi - \langle \psi \rangle)} \rangle$. Using the inequality $\langle e^{\beta\psi} \rangle \geq e^{\beta\langle \psi \rangle}$ one sees that Δs_{SW} is always negative or zero, and thus $-T \Delta s_{SW}$ adds positively to $\mu_{ex,S}$. For molecules with attractive interactions Δu_{SW} is always negative. Negative values of $\mu_{ex,S}$ therefore always result from favorable solute–solvent interactions $\Delta u_{SW} < 0$ overriding the solute–solvent entropy. We note that $-T \Delta s_{SW}$ may be interpreted as the work of creating a cavity that has the solvent molecules in the appropriate positions and orientations to accommodate all chemical moieties of the solute; Δu_{SW} is the interaction energy of the solute with the properly formed cavity. The quantity $\exp[\Delta s_{SW}/k_B]$ is the probability to observe the above cavity in configurations of the pure solvent.

The (constant pressure) excess partial molar enthalpy ($h_{ex,S}$)_P contains, in addition to the solute–solvent energy Δu_{SW} , a contribution arising from changes of solvent–solvent interactions. This contribution is different depending on whether the pressure or volume is kept fixed.^{19,20} At constant pressure, the solvent–solvent energy (enthalpy) change is denoted $(\Delta h_{WW})_P = (\Delta u_{WW})_P + p \Delta v \approx (\Delta u_{WW})_P$. This energy change is localized in the solute hydration shell unlike in the constant volume case where it includes a nonlocal bulk response contribution.^{19,20} Below we will drop the subscript $(\cdots)_P$. One should keep in mind that in this paper excess partial molar enthalpies and entropies are evaluated at constant pressure. Assuming the energies Δu_{SW} and Δh_{WW} are additive yields

$$h_{ex,S} = \Delta u_{SW} + \Delta h_{WW} \quad (10)$$

Because the excess chemical potential is defined as $\mu_{ex,S} = h_{ex,S} - Ts_{ex,S}$, the excess partial molar entropy is given by

$$s_{ex,S} = \Delta s_{SW} + \Delta h_{WW}/T \quad (11)$$

Hence, $h_{ex,S}$ and $Ts_{ex,S}$ contain a contribution (Δh_{WW}) which never impacts $\mu_{ex,S}$ (exact energy-entropy compensation). Although the definitions of Δu_{SW} and Δs_{SW} (eq 9) take slightly different forms in the constant P - T and constant V - T ensembles their values are ensemble-independent.

From eq 9 it can be seen that energy fluctuations $\psi - \langle \psi \rangle > 0$ contribute most significantly to the solute-solvent entropy. To better understand the physics inherent in Δs_{SW} it is useful to think of it as having two contributions of which both are negative. First, Δs_{SW} has a cavity contribution that arises from repulsive solute-solvent interaction energies ($\psi > 0$) with corresponding solvent configurations that violate the excluded volume constraint imposed by the solute. This contribution reflects the tendency of the solvent to close the solute cavity (or “squeeze-out” the solute). The second contribution arises from fluctuations of the interaction energy in configurations where the interaction is attractive ($\psi \leq 0$). Sanchez et al.³⁷ derived

$$\begin{aligned} \Delta s_{SW}/k_B &= \ln P_{ins} - \ln \langle e^{\beta(\psi - \langle \psi \rangle)} \rangle_a - \ln P_a \\ &= \ln P_{ins} - [(\langle \psi^2 \rangle - \langle \psi \rangle^2)\beta^2/2 + \dots]_a - \ln P_a \quad (12) \end{aligned}$$

where the subscript ‘a’ indicates that the average is taken under the condition that the solute-solvent interaction energy is attractive ($\psi < 0$). The quantity P_{ins} is the probability that a randomly inserted solute molecule into a system of only solvent molecules will experience an attractive or zero interaction ($\psi \leq 0$). P_a is the probability that the solute molecule in the fluid will have an attractive energy. Because P_a will be very close to unity the $\ln P_a$ term can be ignored. The second term on the right-hand side of eq 12 will always be zero in case ψ is independent of the positions and orientations sampled by solvent molecules vicinal to the solute. In a mean field approximation, where fluctuations in the energy are ignored, this term would actually be set to zero and $\Delta s_{SW}(= k_B \ln P_{ins})$ would then be determined by the cavity contribution only. Thus, in a mean field approximation, one would only account for excluded volume effects and the corresponding loss of solvent translational entropy. In eq 12, the fluctuation term $(\langle \psi^2 \rangle - \langle \psi \rangle^2)\beta^2/2$ expresses the fact that the available configuration space is biased by attractive interactions (i.e. solute-solvent attractive interactions bias positions and orientations of the vicinal solvent molecules). The corresponding loss of configuration space causes a loss of entropy.

References

- (1) Murphy, K. P.; Privalov, P. L.; Gill, S. J. *Science* **1990**, *247*, 559.
- (2) Hummer, G.; Garde, S.; García, A. E.; Paulaitis, M. E.; Pratt, L. R. *J. Phys. Chem. B* **1998**, *102*, 10469.
- (3) Dill, K. A. *Biochemistry* **1990**, *29*, 7133.
- (4) Hummer, G.; Garde, S.; García, A. E.; Paulaitis, M. E. *Proc. Natl. Acad. Sci. U.S.A.* **1998**, *95*, 1552.
- (5) Southall, N. T.; Dill, K. A.; Haymet, A. D. J. *J. Phys. Chem. B* **2002**, *106*, 521.
- (6) Frank, H. S.; Evans, M. E. *J. Chem. Phys.* **1945**, *13*, 507.
- (7) Makhataдзе, G. I.; Privalov, P. L. *Biophys. Chem.* **1994**, *50*, 285.
- (8) McAuliffe, C. J. *J. Phys. Chem.* **1966**, *70*, 1267.
- (9) Makhataдзе, G. I.; Privalov, P. L. *J. Solution Chem.* **1989**, *18*, 1267.
- (10) Makhataдзе, G. I.; Privalov, P. L. *J. Mol. Biol.* **1990**, *213*, 375.
- (11) Levitt, M.; Perutz, M. F. *J. Mol. Biol.* **1988**, *201*, 751.
- (12) Linse, P. *J. Am. Chem. Soc.* **1990**, *112*, 1744.
- (13) Atwood, J. L.; Hamada, F.; Robinson, K. D.; Orr, G. W.; Vincent, R. L. *Nature* **1991**, *349*, 683.
- (14) Suzuki, S.; Green, P. G.; Bumgarner, R. E.; Dasgupta, S.; Goddard, W. A., III; Blake, G. A. *Science* **1992**, *257*, 942.
- (15) Jorgenson, W. L.; Severance, D. L. *J. Am. Chem. Soc.* **1990**, *112*, 4768.
- (16) Graziano, G.; Lee, B. *J. Phys. Chem. B* **2001**, *105*, 10367.
- (17) Ben-Naim, A.; Marcus, Y. *J. Chem. Phys.* **1984**, *81*, 2016.
- (18) Yu, H.-A.; Karplus, M. *J. Chem. Phys.* **1988**, *89*, 2366.
- (19) Matubayasi, N.; Reed, L. H.; Levy, R. M. *J. Phys. Chem.* **1994**, *98*, 10640.
- (20) Levy, R. M.; Gallicchio, E. *Annu. Rev. Phys. Chem.* **1998**, *49*, 531.
- (21) Lee, B. *Biopolymers* **1985**, *24*, 813.
- (22) Brooks, C. L., III; Karplus, M.; Pettitt, B. M. In *Advances in Chemical Physics*; Prigogine, I., Rice, S. A., Eds.; 1988; Vol. 71.
- (23) Lindahl, E.; Hess, B.; van der Spoel, D. *J. Mol. Model.* **2001**, *7*, 306.
- (24) Berendsen, H. J. C.; van der Spoel, D.; van Drunen, R. *Comput. Phys. Commun.* **1995**, *91*, 43.
- (25) Berendsen, H. J. C.; Postma, J. P. M.; van Gunsteren, W. F.; Hermans, J. in *Intermolecular Forces*; Pullman, B., Ed.; Reidel: Dordrecht, 1981; pp 331-342.
- (26) van Gunsteren, W. F.; Billeter, S. R.; Eising, A. A.; Hünenberger, P. H.; Krüger, P.; Mark, A. E.; Scott, W. R. P.; Tironi, I. G. *Biomolecular Simulation: The GROMOS96 Manual and User Guide*; vdf Hochschulverslag: ETH Zürich, Switzerland, 1996.
- (27) Oostenbrink, C.; Villa, A.; Mark, A. E.; Van Gunsteren, W. F. *J. Comput. Chem.* **2004**, *25*, 1656.
- (28) Berendsen, H. J. C.; Postma, J. P. M.; van Gunsteren, W. F.; DiNola, A.; Haak, J. R. *J. Chem. Phys.* **1984**, *81*, 3684.
- (29) Ryckaert, J.-P.; Ciccotti, G.; Berendsen, H. J. C. *J. Comput. Phys.* **1977**, *23*, 327.
- (30) Karlström, G.; Linse, P.; Wallqvist, A.; Jönsson, B. *J. Am. Chem. Soc.* **1983**, *105*, 3777.
- (31) Linse, P.; Karlström, G.; Jönsson, B. *J. Am. Chem. Soc.* **1984**, *106*, 4096.
- (32) Postma, J. P. M.; Berendsen, H. C.; Haak, J. R. *Faraday Symp. Chem. Soc.* **1982**, *17*, 55.
- (33) Gallicchio, E.; Kubo, M. M.; Levy, R. M. *J. Phys. Chem. B* **2000**, *104*, 6271.

- (34) Gill, S. J.; Dec, S. F.; Olofsson, G.; Wadsö, I. *J. Phys. Chem.* **1985**, 89, 3758.
- (35) Lee B. *Biophys. Chem.* **1994**, 51, 271.
- (36) Stone, M. T.; In 't Veld, P. J.; Lu, Y.; Sanchez, I. C. *Mol. Phys.* **2002**, 100, 2773.
- (37) Sanchez, I. C.; Truskett, T. M.; In 't Veld, P. J. *J. Phys. Chem. B* **1999**, 103, 5106.
- (38) Widom, B. *J. Chem. Phys.* **1963**, 39, 2808.

CT049841C